UNIVERSITY of CALIFORNIA
SANTA CRUZ

TRACKING THE RHESSI ZERO-CHANNEL ENERGY USING A 10.2 KEV BACKGROUND FEATURE

A thesis submitted in partial satisfaction of the
requirements for the degree of

BACHELOR OF SCIENCE

in

PHYSICS

by

Karl Schmidt

31 May 2010

The thesis of Karl Schmidt is approved by:

Professor David M. Smith
Advisor

Professor David P. Belanger
Senior Theses Coordinator

Professor David P. Belanger
Chair, Department of Physics

Abstract

Tracking the RHESSI Zero-Channel Energy Using a 10.2 keV Background Feature

by

Karl Schmidt

The field of solar physics is intrinsically limited by remote observing and indirect measurements. Satellites, such as the Reuven Ramaty High Energy Solar Spectroscopic Imager (RHESSI), are expensive, therefore maximizing accuracy extends the lifetime and maximizes scientific value. The dominating term in the RHESSI calibration function at low energy is the zero-channel energy (offset). Fluctuations in the offset affect the analysis of the iron fluorescence feature at 6.7 keV, near the lower bound of RHESSI's sensitivity. Iron fluorescence is an important diagnostic of plasma temperatures associated with solar flares.

The offset was found to fluctuate on two time scales: the period of an orbit and over several days. Over an orbital cycle the offset decreased 0.03 keV; the best found fit was a second-order, concave-down polynomial. The cause of this variation not identified specifically. Over the course of fifteen orbits the offset fluctuates sinusoidally by $\sim$0.1 keV due to the interaction with the South Atlantic Anomaly (SAA). The period of the sine deviated from the predicted value of the Earth's rotation and satellite precession interaction by 0.3 percent. Correcting for these fluctuations allows higher accuracy in RHESSI's low energy range.

Contents

1

Introduction

1.1 The Sun

Ninety three million miles from Earth the Sun's interior dynamo produces magnetic fields, thousands to millions of times stronger than the magnetic fields on Earth. The Sun's high temperatures from gravitational compression and nuclear fusion strip electrons from nuclei creating plasma. The magnetic fields exert a lorentz force on moving charged particles and plasma flows produce magnetic fields. These forces create and destroy magnetic field and accelerate plasma.

Inside the Sun the particle pressure is immense compared to the magnetic field pressure ($B^2/2\mu$) (Aschwanden 2005). The motions and flows of the plasma dominate and the magnetic fields are dragged along for the ride. Conversely, the solar corona is diffuse; the particle pressures are lower than the best vacuums humans can create on Earth (Aschwanden 2005). Where the particle pressure is low, the magnetic field pressure dominates and the particles follow the magnetic fields–often in elegant loops protruding from the more dense

layers of the Sun.

The dominating pressure –magnetic or particle– plays a key role in the production of solar flares. The ratio of these two pressures is refered to as the plasma beta parameter and is a useful way to characterize a region. Below the transition between the dominating pressures the particle pressure moves the loops around, but above the transition layer the plasma filled loops resist the movement. Magnetic fields in a vacuum can move with the flow, but because the magnetic fields contain plasma they have inertia and resist the change. Contours of constant magnetic field cannot cross so the magnetic field becomes tangled. Analogous to rubber bands, the tangled configuration is a higher energy configuration; at some point the energy is released in an event known as a solar flare.

Reconnection is the process of the twisted fields snapping to a lower energy configuration and releasing the difference in energy. Reconnection involves magnetic field contours reconfiguring so that they remain continuous but are no longer tangled, (Aschwanden 2005). Energy is released by accelerating the particles in the plasma, which follow the magnetic fields down to the surface, or chromosphere (Aschwanden 2005). The accelerated plasma heats up the chromosphere around the footpoints of the flare loop causing electrons and protons to evaporate up into the outer region where the magnetic field dominates, the corona. The evaporated particles interact with each other emitting X-rays (Priest 2000).

Bremsstrahlung –free-free emission– is the high velocity coulomb interaction between an electron and ion that produces X-rays. An electron or proton is elastically scattered and the change in kinetic energy is the energy of the emitted photon (Aschwanden 2005). The distribution of X-rays produced reflects the distribution of particle energies. The plasma that evaporates into the flare loops has a thermal distribution of energies (Aschwan-

den 2005) up to ∼10 keV (Phillips et al. 2006) and higher in larger flares. Large solar flares also produce X-rays from a non-thermal distribution of plasma energies by Bremsstrahlung (Aschwanden 2005).

X-rays are also produced by heavier ion fluorescence as a result of the accelerated particle bombardment. Iron (Fe), present in the photosphere, chromosphere and the corona, produces a fluorescence complex in the soft X-ray range ∼6.7 keV (Phillips et al. 2006). The distribution of ionization states is temperature dependent; at higher temperatures Fe is likely to have less electrons. With less electrons the coulomb force is less screened and the binding energy increases, resulting in higher photon energy from stimulated emission. The highest energy fluorescence, from higher ionization states of Fe, is emmitted from regions with temperatures ∼9-12 $\times 10^6$ K (Doschek 2000). The peak of the iron fluorescence feature is used as a diagnostic of the electron temperatures of x-ray producing regions and thus the temperatures corresponding to solar flares (Phillips et al. 2006).

1.2 Instrument

The Reuven Ramaty High Energy Solar Spectroscopic Imager (RHESSI), was launched in February 2002 and has provided solar flare spectra and images with an energy sensitivity from ∼3 keV to ∼17 MeV (Phillips et al. 2006). The detectors are segmented into a front and rear sections to prevent the rear detectors, where gamma-rays are detected, from being saturated by more abundant thermal X-rays (Smith et al. 2000). The front segments are 1 cm thick, have a spectral resolution of ∼1 keV FWHM and are sensitive up to about 300 keV (Smith et al. 2000).

RHESSI's nine segmented detectors are made out of germanium. The germanium

is maintained at cryogenic temperatures of about 80 K–now about 100K–by an onboard cooling system (Smith et al. 2000). At this temperature the germanium is an electrical insulator; there are no electron-hole pairs in the conduction band. When an X-ray or gamma-ray is incident on the detector it transfers its energy to an electron in the lattice. The energetic electron creates an ionization trail as it moves through the germainium producing electron-hole pairs in the conduction band. A potential of up to 4 kV is applied across the detector by the onboard power-supply (Lin et al. 2002). The electrons and holes feel a force toward opposite electrodes, thus the incident particle creates a measurable current pulse (Smith et al. 2000).

Current pulses can be analyzed because incident particles create pulses proportional to their energy (Smith et al. 2000). The current pulses go to the charge sensitive pre-amplifier where the signals are amplified by an amount proportional to photon energy. The signal is then passed to the Instrument Data Processing Unit (IDPU) where it is shaped and amplified and the peak detected and converted to a digital signal. The signal is designated to one of 8192 channels and is then stored in the onboard memory until the information can be telemetered to the ground (Lin et al. 2002).

Material properties, such as the resistance of resistors and wires and the capacitance of capacitors (capacitance is dependent on the dimensions of the capacitor components), are temperature dependent. The temperature on the spacecraft fluctuates as it passes from night to daytime. Charged particles and cosmic rays incident on the spacecraft can effect small changes in voltages. High fluences of charged particles are encountered periodically in RHESSI's orbit and may alter the functionality and sensitivity of the electronics.

Cosmic rays incident on the Earth's atmosphere produces high energy neutrons. The lack of coulomb forces allows high energy neutrons to penetrate the protective layers surrounding the detectors. These neutrons' high kinetic energy disorders the germanium crystal when it collides with a germanium nuclei. Disorder in the crystal acts as hole traps, reducing the signal pulse generated by subsequent X-ray incidence. Once holes are trapped the electric field in the crystal shifts and the detector resolution decreases.

The relationship between channel number and photon energy is the "gain function." The gain function is determined using spectral lines–93.3 keV and 511 keV. For the front detectors the formula is approximately: Energy = ($\sim$0.33 keV ch^{-1}) $\times$ channel - 12 keV.

Fluctuations in the physical properties of the electronics can vary the terms in the gain formula causing inaccurate conversions. For incident particles on the low end of RHESSI's range the channel is low and the gradient, or gain, is a small component of the resulting energy; whereas the zero-channel energy, or 'offset,' plays a larger role in the energy conversion.

According to Phillips et al. (2006) the advantage of measuring the Fe feature at $\sim$6.7 keV with RHESSI is the simultaneous measure of the continuum emission and the Fe feature. The electron temperature is derived from the ratio of the Fe emission to the continuum flux (Phillips et al. 2006). The spectral resolution of RHESSI at these energies is 1 keV, much less than that of a Bragg Crystal Spectrometer (such as the one on satellite Yohkoh) which can see the fine line structure of the Fe feature, but not measure the background continuum (Phillips et al. 2006). The Fe feature also reveals the extent of the thermal distribution which connects to a power-law distribution of accelerated electron

energies. The Fe feature shows up at low end of RHESSI's energy sensitivity where the offset is a significant percentage of the calculated energy. Small fluctuations in the offset affect the analysis of the Fe fluorescence feature.

Just above the 6.7 keV Fe feature RHESSI observes an emission line at 10.2 keV. The 10.2 keV line is not produced by the Sun as RHESSI observes this line during the night. The origin of the line is yet unknown but it is a useful calibration tool at low energies.

1.3 South Atlantic Anomaly

The Earth's magnetic field is not a symmetric dipole field, consequently a region located above South America traps charged particles in the orbital path of RHESSI. The South Atlantic Anomaly, or SAA, is a region where the magnetic flux through the surface of the Earth is minimum and the charged particle flux is maximal (Heirtzler 2002). In this region the Van Allen Radiation belts extend down to the atmosphere, 100 km from the Earth's surface (Heirtzler 2002). In this region protons and electrons are mirroring in the magnetosphere. Spacecraft passing through can suffer from "single event upset" (SEU) where a single particle causes an equipment malfunction (Heirtzler 2002). The radius of RHESSI's orbit is within the reaches of the SAA and, due to Earth's daily rotation, approximately six of fifteen daily orbits include a pass through the SAA.

During an SAA pass RHESSI does not record data. The flux of charged particles is significantly higher than that coming directly from the Sun; the detectors are heavily saturated and unable to make precise observations. The detectors and electronics on the satellite may be affected by the increased flux of charged particles. The SAA is a possible cause of offset fluctuations.

1.4 Calibration Project

The aim of this project was to identify and characterize trends in the fluctuation of the zero-channel energy, or offset, of the RHESSI gain formula using the 10.2 keV emission line. The offsets was tracked over two time periods: one orbital period, and 63-165 consecutive orbits. From the start of the mission some of RHESSI's detectors have operated with higher resolution than others (Smith et al. 2000). An energy resolution of $\sim$1 keV is necessary to study the Fe fluorescence feature (Phillips et al. 2006) therefore only the front segments of detectors 1, 3, 4, 6, 8 and 9 were investigated in this project.

2

Methods

2.1 Identifying Low X-ray Flux Time Ranges

The first goal was to identify periods of time longer than three days, within the first two years of the RHESSI mission, where the solar X-ray flux was below 10^{-6} W/m^2, according to GOES –The Geostationary Operational Environmental Satellite– data (http://www.oso.noaa.gov/goes/). GOES is a system of satellites set up to monitor the environment on Earth as well as in space.The RHESSI Browser (http://sprg.ssl.berkeley.edu/ tohban/browser/) is an online database that displays solar X-ray flux measurements from GOES alongside RHESSI spectroscopic data. The GOES data are marked with RHESSI eclipse times as well as SAA times.

The time ranges with low background count rates were chosen because the 10.2 keV line could not be resolved when the Sun was active. The Sun was coming out of the sunspot maximum–an eleven year cycle (Aschwanden 2005)–at the start of the mission, making this a difficult criterion to meet. Six time ranges fitting the criterion and longer

Table 2.1: Time Ranges

Start Time	Stop Time	Number of Orbits
2002-Jun-12 22:00:00	2002-Jun-19 08:00:00	96
2002-Dec-26 10:00:00	2002-Dec-30 18:00:00	63
2003-Feb-23 00:00:00	2003-Feb-28 00:00:00	75
2003-May-09 03:00:00	2003-May-19 21:45:00	161
2003-Aug-31 12:00:00	2003-Sep-11 13:00:00	165
2003-Oct-10 00:00:00	2003-Oct-18 03:00:00	122

than three days were found. The time ranges ranged from three to eleven days.

2.2 Obtaining Photon Data

The photon data for the time ranges in Table 2.1 were collected using standard RHESSI software in five-minute increments. The format of the data was the accumulation of counts over five minute increments. Before the data were requested the time segments that include an SAA pass were flagged, no data was stored while the satellite was in the SAA but these orbits were marked to explore the affect of the SAA on the gain function. The data were stored in an array with dimensions 16 by 18 by 8192. The dimensions represent the five minute portion of the specific orbit, the detectors, and the counts in each channel respectively.

2.3 Tracking the Offset Over Consecutive Orbits

An IDL procedure was created to plot the offset paramter each orbit for 63 to 165 consecutive orbits. For each orbit in the specified time range, the counts for all the five minute segments of that orbit were summed. The 10.2 keV feature was fit to find the channel corresponding to the peak.

2.3.1 Fitting the 10.2 keV Line

The 10.2 keV line was fit with the sum of a gaussian and a quadratic , Eq. 2.1, using the "mpfit" (Markwardt 2008).

$$f(x) = A + Bx + Cx^2 + n \exp\left(-\frac{0.5(x - x_0)^2}{\sigma^2}\right) \tag{2.1}$$

Estimates of the fitting parameters were fed to the fitting procedure. The fitting procedure updated these terms until they converge and the χ^2 was minimized (Markwardt 2008). The fitted center channel (x_0) was assigned an energy of 10.2 keV and an offset was determined using Eq. 2.2. The gain for each five-minute segment was determined by standard RHESSI software, the arithmetic mean of the gains was used to calculate the offset.

$$Energy = Offset + (Gain)(Channel\#) \tag{2.2}$$

Or

$$Offset = 10.2keV - (Gain)x_0 \tag{2.3}$$

The offsets were plotted and the orbits including an SAA pass were marked to identify any correlations.

2.3.2 Finding the Period of Daily Offset Oscillations

The period of the daily oscillations was visually close to the period of one day, 8.6×10^4 seconds, so a computer program was written to find the period. First a linear fit was found and removed in order to focus on the sinusoidal variations subtracted. The

offsets were folded over each other at varying periods using Eq. 2.4.

$$\phi = \frac{2\pi(t - t_0)Modulus(T)}{T} \tag{2.4}$$

Where the phase ϕ was determined for each offset by the difference between the initial time and that time multiplied by the modulus of the period (T) and divided by the period. The folding period was increased by 300 seconds from 7.3×10^4 to 9.4×10^4 seconds and Eq. 2.4 assigned a fraction of a 2π radian cycle to each point in relation to the initial point. A mean of the offsets with same phase was taken. Chi-squares for the mean offsets for each phase were calculated with respect to the overall mean offset. The goal was to maximize χ^2 and thus reveal the period at which the amplitude of the sine is maximal.

The χ^2 vs. period was fit with a lorentzian (Eq. 2.5) using the fitting routine mentioned earlier, mpfit (Markwardt 2008).

$$L(t) = N\frac{\sigma}{\pi((t - t_0)^2 - \sigma^2)} \tag{2.5}$$

where the lorentzian was a function of period. The fitted center of the lorentzian is used as the starting value for the period when the fitting routine –mpfit–is run with a sine function on the offsets using Eq. 2.6.

$$S(t) = -A\sin(tT + \delta) \tag{2.6}$$

2.4 Tracking the Offset Over an Orbital Period

We first aligned the five minute segments composing each orbit, starting from sunrise, then summed the data corresponding to the segments fifteen orbits at a time, or twenty four hours at a time. Each summed five minute segment was normalized by the

number of segments composing it because not all orbits contain the same number of five minute segments.

For each five minutes of the composite orbit, the low energy spectral line around 10.2 keV was fit with a gaussian and a parabola as previously decscribed. The fitted center channel of the gaussian was used as the 10.2 keV channel. The offset is related linearly to the gain (see Eq. 2.3) so the fitted center channel of the 10.2 keV line was followed instead of the offset.

To determine if there was a relationship between the offsets and the background count rate, the reduced χ^2 of a linear regression was determined for two data sets: all of the offsets and the ninety percent of the offsets with the lowest background counts. The background counts were measured at the 6.0 keV channel using Eq. 2.7. Also the fitted-center channels for each time range and each detector were combined by subtracting the mean of each subset, and a line was fit.

$$6keVchannel = \frac{(10.2keV - 6.0keV)}{gain} + x_0 \tag{2.7}$$

where x_0 is the fitted center of the 10.2 keV line.

The χ^2 were calculated between the fitted-center channel of the 10.2 keV line and the linear fit.

The error was estimated with the root mean square (RMS) from the average in each five minute segment.

$$\sigma^2 = \frac{\sum_{i=1}^{g}(c_g - \bar{c})^2}{g} \tag{2.8}$$

where "g" was the number of offsets (one for each 24 hour day) at that five-minute segment, "c_g" was the offset, and "$\bar{c}$" was the mean of all c_gs.

3

Results and Analysis

3.1 Fitting the 10.2 keV Spectral Line

The aim was to fit a guassian plus a second-order plynomial to the emission line between channels 50 and 80 and assign the fitted center channel to the energy 10.2 keV. Fitting a gaussian plus a quadratic to the low energy spectral line provided the energy bin corresponding to the 10.2 keV line. The background counts were produced by the instrument, the Earth's atmosphere and the Sun; the exact function was unknown and shifting. Any function can be expanded as a series of polynomials according to Taylor's theorem. The background was continuous and smooth and was therefore approximated with a second-order polynomial. The third order could have produced a bump where the spectral line was so the polynomial series was truncated at second-order and a gaussian was added for the emission line itself.

When the Sun is active it has a thermal emission spectrum; Planck's Law gives the form of the energy distribution for a blackbody as the Maxwell-Boltzman (Tipler et al.

2002) distribution, see Eq. 3.1.

$$f(E) = A \exp\left(-\frac{E}{kT}\right) \tag{3.1}$$

The series expansion of an exponential, equation below, converges for all values in the domain.

$$f(E) = e^x = 1 + x + \frac{x^2}{2!} + \frac{x^3}{3!} + \tag{3.2}$$

Dropping terms higher than second order approximates the background energy distribution as a second order polynomial. Therefore a second-order polynomial was appropriate for the background at varying amounts of solar activity.

3.2 The Sinusoidal Period of the Daily Offset

We saw that the offset had a period of about one Earth day, 86400 seconds (see Fig. 3.2). The aim was to see if the period observed was exactly one day or less than one day, and to see where the orbits including an SAA interaction lie. At low energies fluctuations in the offset change the energy by a greater percent than any deviation in the gain because the gain is scaled by the channel of the incident photon. The offset fluctutated by +/- 0.05 keV. The fluctuations were sinusoidal.

Orbits containing the SAA appeared at constant phase of the sinusoid, see Fig. 3.2. The precessional period of the satellite is approximately 61 Earth days or 915 orbits. For the SAA to cause the sinusoidal pattern the period must be related to the precessional period. Other fixed points on Earth could cause the trend such as changes in the Earth's surface reflectivity (albedo). The aim was therefore to determine the period of the sinusoid.

The fit of the chi-squares vs. period was closer to a lorentzian than a gaussian and

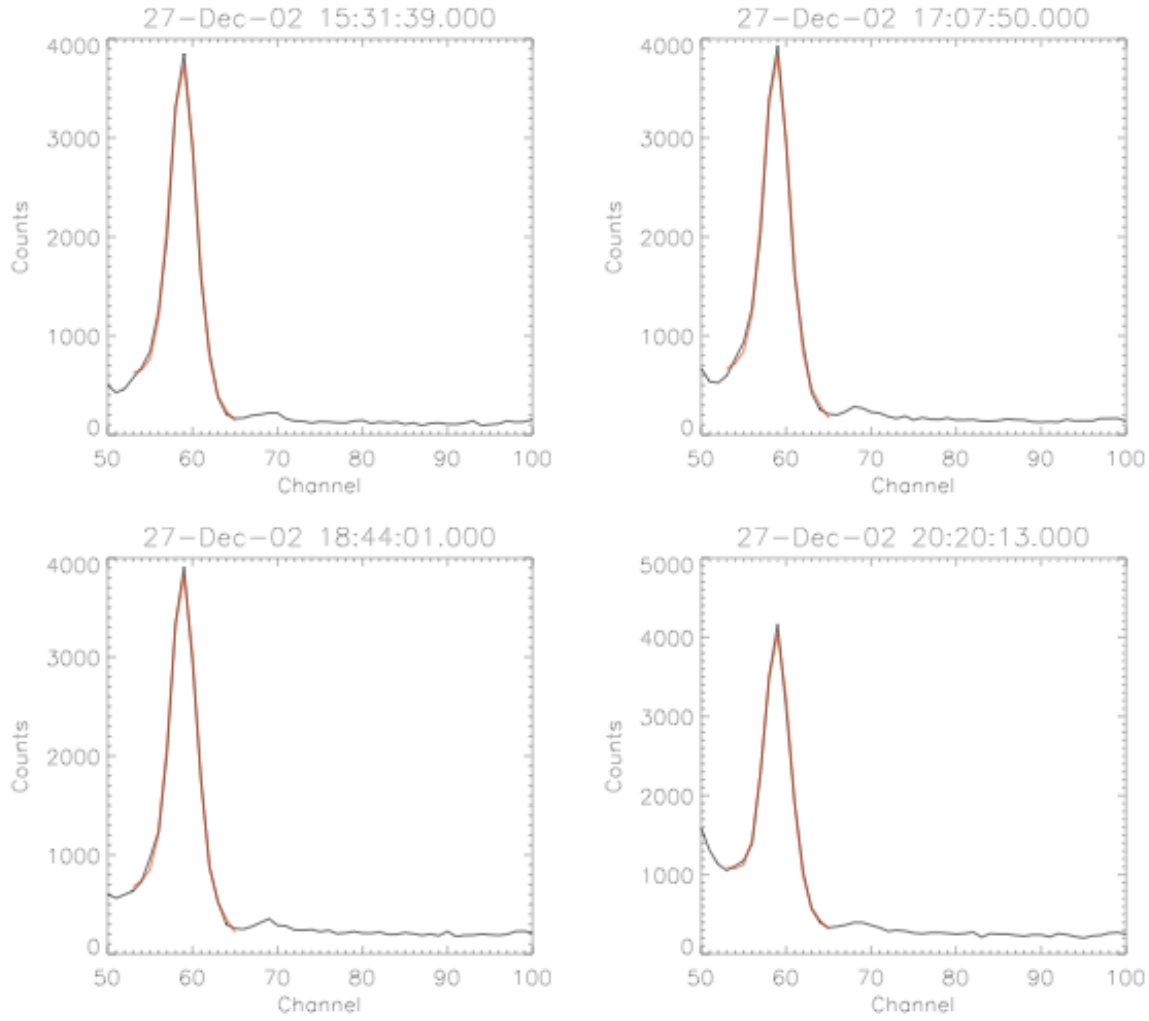

Figure 3.1: Fitted gaussian plus quadratic (red line) over 10.2 keV spectral line for four consecutive orbits. These plots show orbits from the December 2002 time range and data from detector 9.

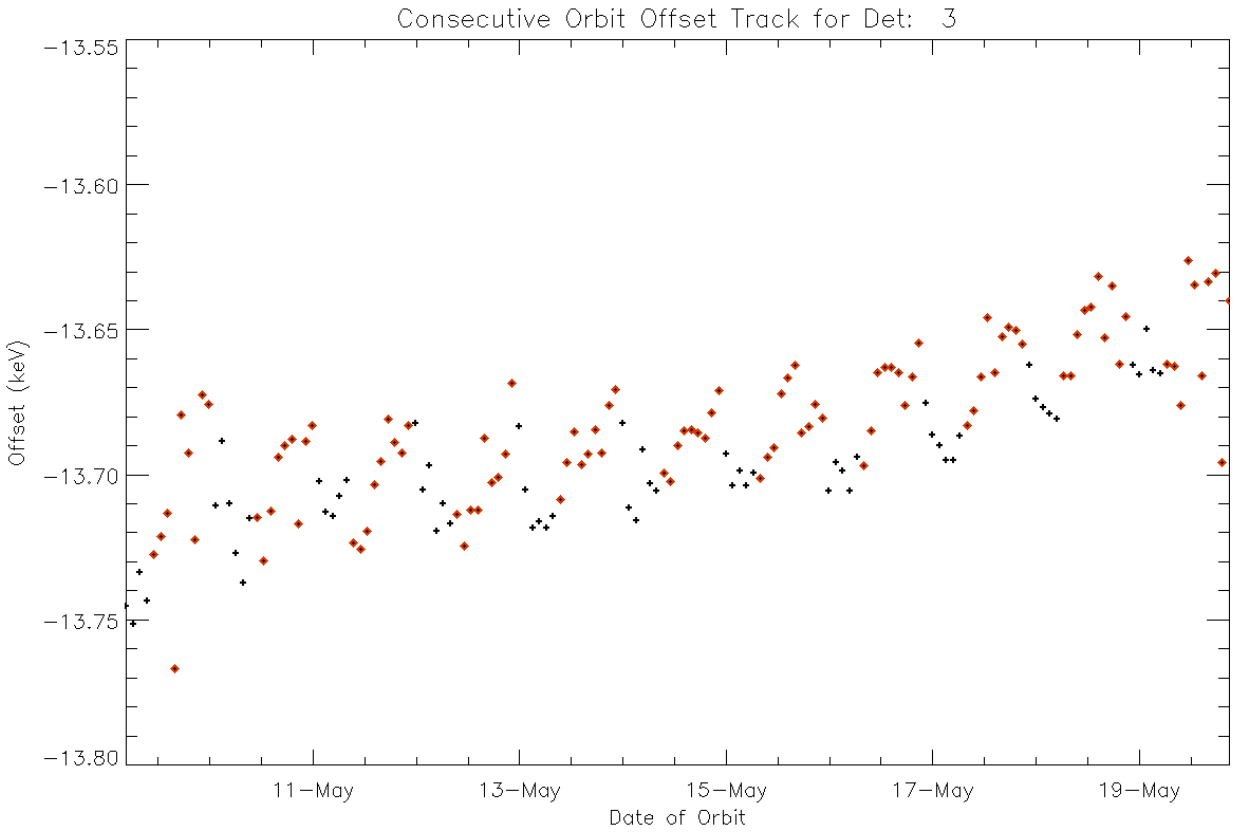

Figure 3.2: Offset for May 2003 time range. The orbits including an SAA pass are marked with red.

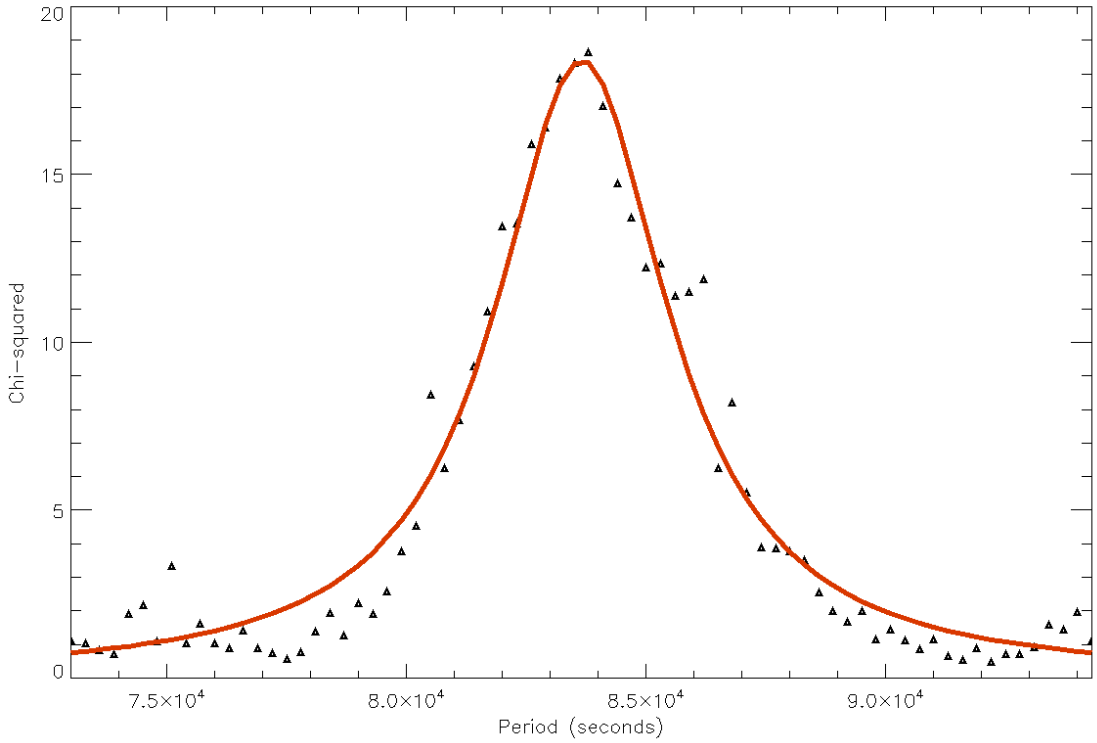

Figure 3.3: Lorentzian fitted to χ^2 at varying fold periods of the consecutive orbit track. Note the period of the the Earth's rotation lies at $8.64\times10^4 s$, just above the peak of the most probable period of the fluctuation. This plot is of the May 2003 time range with detector 3, see Fig. 3.2.

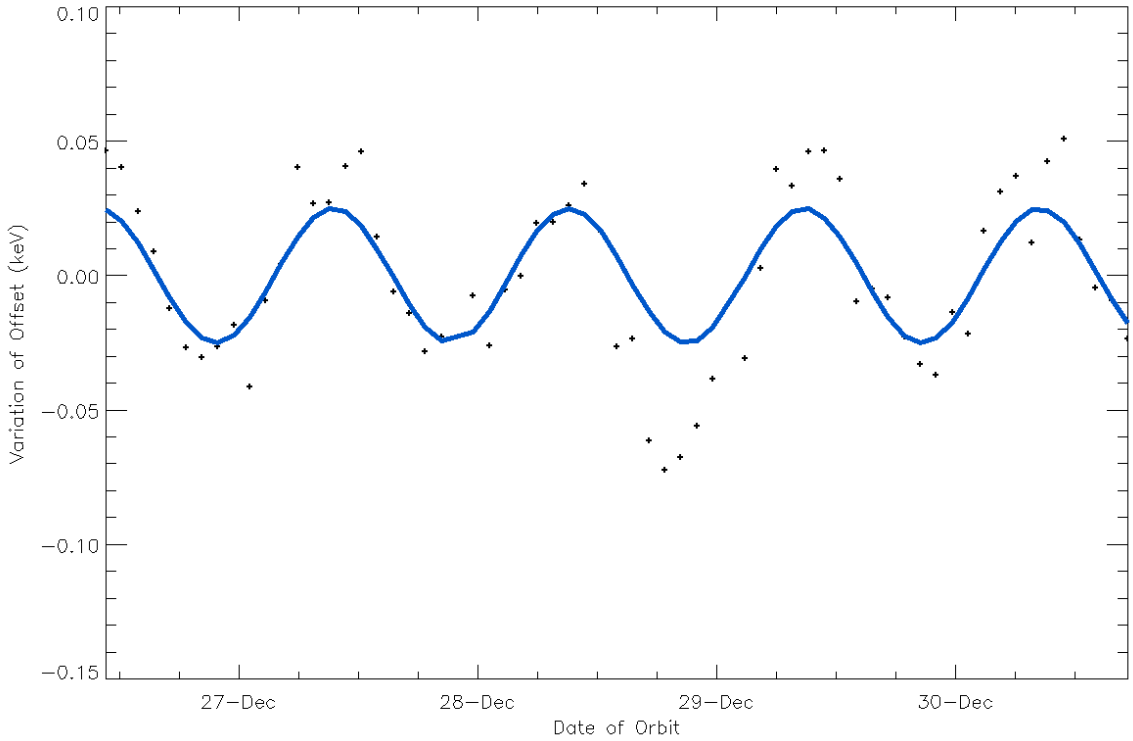

Figure 3.4: The fitted sine over offset variations for detector 1 during the December 2002 time range. The reduced χ^2 for this fit was 0.02.

the fitted center was to be used as a starting estimate in the fitting of the sinusoid, see Fig. 3.2. Where the chi-square was maximal the pattern was least like a constant.

The fit periods were consistently less than the period of one day. If the satellite had an equatorial orbit and did not precess the satellite would fly over the SAA, or other fixed points on Earth, exactly every Earth rotation, 86400 seconds. From the stellar reference frame the angular position of the satellites interaction with a fixed point on Earth is the sum of the fixed point's position and the satellite orbital position: $\Theta = \theta_{Earth} + \theta_{Satellite}$. Thus the angular velocity is the time derivative of the angular position:

$$\frac{d\Theta}{dt} = \frac{d\theta_{Earth}}{dt} + \frac{d\theta_{Satellite}}{dt} \tag{3.3}$$

Table 3.1: Mean Periods

Detector	Mean Period	Mean Difference: (86400s - Mean Period)
Earth Day	8.64	0
Beat period	8.50	0.144
1	8.44	0.200
3	8.45	0.188
4	8.46	0.180
6*	8.52	0.118
8*	8.53	0.109
9	8.45	0.189
Mean	8.48	0.164

All times in 10^4 seconds

* The starred averages neglected the May time period because the sinusoidal pattern was unrecognizable, the source of this discrepancy was unknown.

The period of the offset was the period of the interaction observed by the fixed stars.

$$\frac{2\pi}{T_{Offset}} = \frac{2\pi}{T_{Earth}} + \frac{2\pi}{T_{Satellite}} \tag{3.4}$$

$$T_{Offset} = \frac{T_{Earth}T_{Satellite}}{T_{Earth} + T_{Satellite}} \tag{3.5}$$

Substituting the satellite period ($T_{Satellite}$) of 61 Earth days or $61T_{Earth}$ reduces Eq. 3.5 to $T_{Offset} = \frac{61}{62}T_{Earth}$. The predicted period of the offset if affected by the SAA would be (0.98)(86400s) = 84980s.

As seen in Table 3.1 the average cycle duration –period– fit for the time ranges was 84750s. The mean period of the offset variation differs from the predicted period by 0.3%. Thus some fixed location or series of locations on Earth's surface is causing the sinusoidal offset variation observed. The SAA is one physical link between the Earth's rotation and the satellite's precession; another is the change in surface albedo beneath the satellite.

Water reflects radiation differently than desert, therefore a change in the Earth's surface albedo could variably heat the satellite. Changes in albedo, such as continents surrounded by ocean, are fixed in location on the surface of the Earth, the satellite may be heated cyclically by albedo. The SAA interaction with the germanium may fill the hole traps, briefly alleviating the radiation damage and increasing the size of an X-ray pulse. The high particle flux in the SAA results in a high pulse rate which could increase the temperatures of the onboard electronics. The effects of the SAA are more dramatic than the albedo variations and are likely the cause of the sinusoidal offset pattern.

3.3 The Fit of the Orbital Offset Variation

The aim was to track the fitted centers of the 10.2 keV line over the daylight time in an orbit. Summing the counts from fifteen consecutive orbits by corresponding five minute segments provided enough counts to accurately fit a gaussian to the 10.2 keV emission line. This method also allowed multiple points for each segment of the orbit, easing the estimation of the error with the root mean square (RMS). The center channels were followed for simplicity, they are linearly related to the offset by Eq. 2.3 where the only variant is the fitted center of the 10.2 keV line.

The centers decreased over the average orbit and were fit linearly. The gradient fit for all the time ranges and detectors with subtracted means was -0.006 channels/5-minutes or, approximating the gain as 0.33 keV/channel, about -0.03 keV/orbit. The reduced χ^2 was 1.09. To improve the fit the mean of all the data points in each five minute segment were averaged and the error bars were approximated by the RMS of the variation from the mean. The averages were fit with a second-order polynomial resulting in a closer fit and a

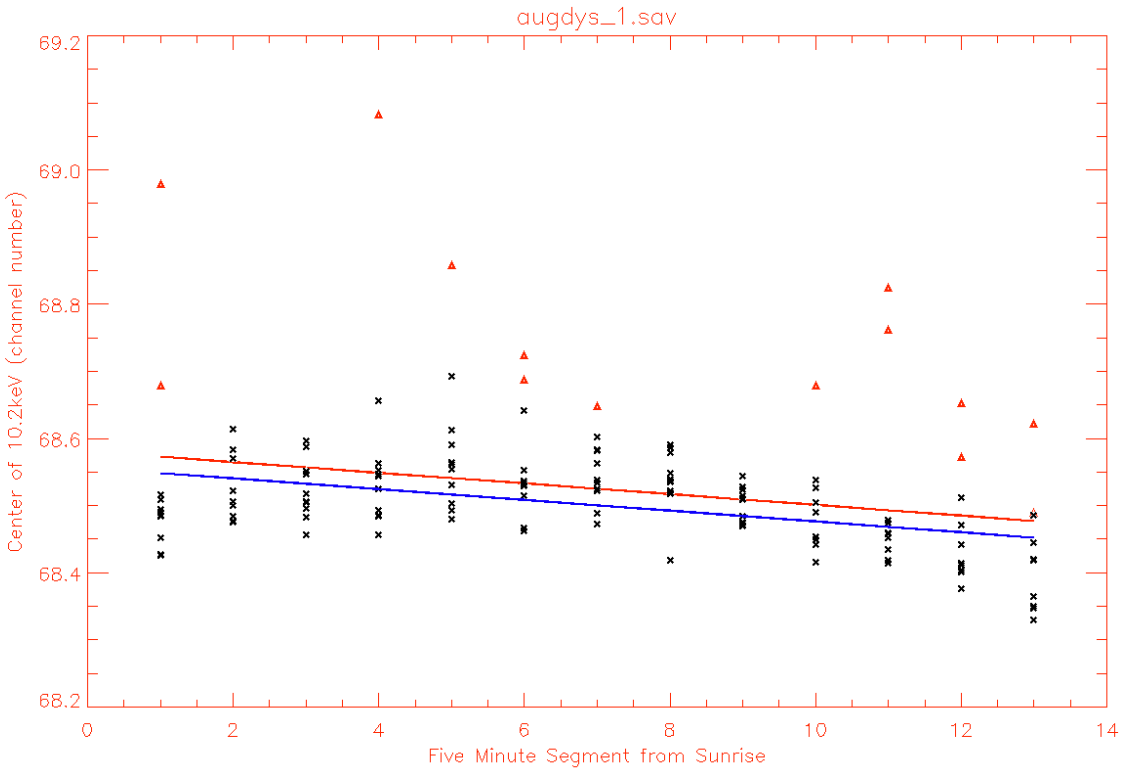

Figure 3.5: Linear fit of 10.2 keV line centers by five minute segment from sunrise. The red triangles are points with the highest background, the red fit is with the red points included and blue fit excludes those points.

χ^2 of 0.5.

The averages of all the centers for each 5-minute segment were also fit with a sinusoid similar to Eq. 2.6 with an added constant; the χ^2 was 0.5. The similarity in fit was expected because a sine is well approximated by a second-order polynomial. The sinusoidal fit was not an improvement in fit. The chi-square was identical to the second-order polynomial and the expense was another free parameter.

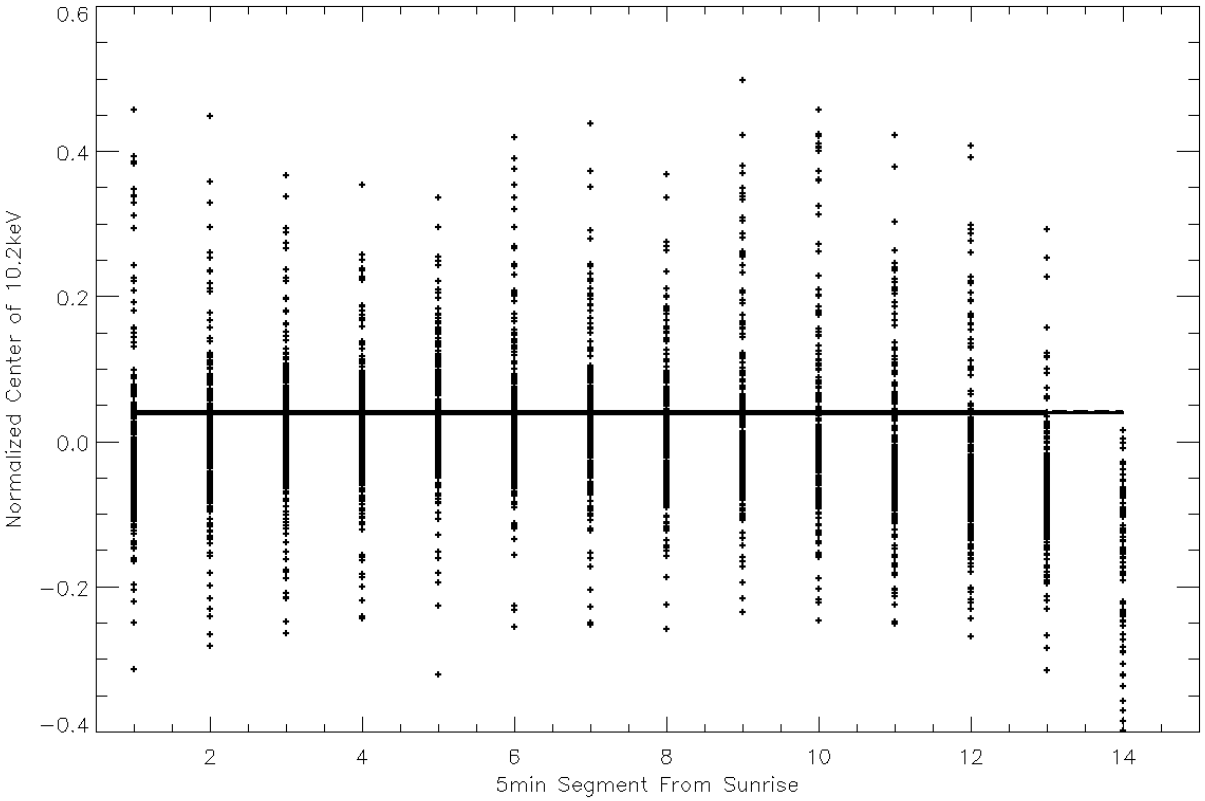

Figure 3.6: Linear fit of all time ranges and all detectors.

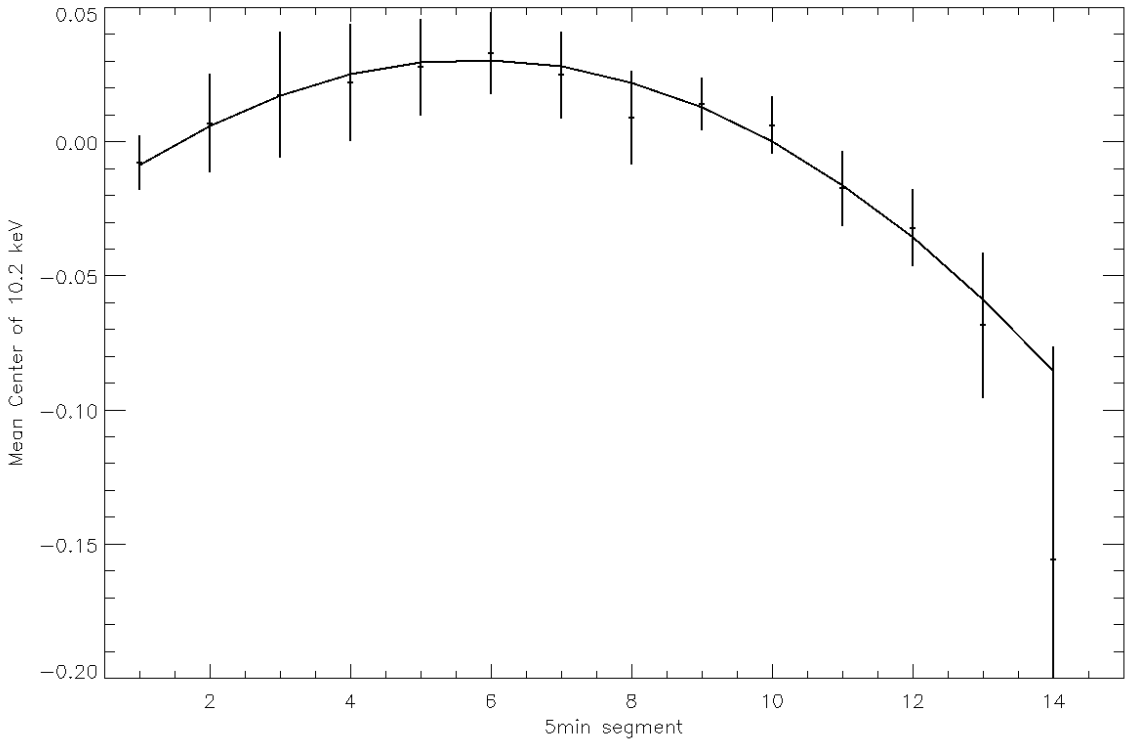

Figure 3.7: Quadratic fit of average fitted center channel over the orbital period. The equation of the line was: $(-0.03 channels) + (0.02 channels/5min)x + (-0.002 channels/5min^2)x^2$. The sinusoidal fit was not plotted because it falls in the exact location of the line shown. The sinusoid equation was: $-1.83 channels + (1.86 channels)\sin((0.043/5min)x + 7.6)$.

4

Conclusions

The peak of the 10.2 keV emission line shifts over the course of an orbit and over longer time periods. The variation was observed in time ranges with solar activity below 10^{-6} W/m^2 by GOES measurements to allow accurate fitting with a gaussian plus a quadratic. The drift of this peak revealed RHESSI's response to the environment; temperature fluctuations as the satellite moves in and out of the sunlight as well as charged particle interactions from passes through the south atlantic anomaly were likely causes of the drift. The drift of the 10.2 keV line also revealed inaccuracies in the RHESSI channel to energy function, or gain function, at the lower end of RHESSI's energy sensitivity.

The offset represents the energy corresponding to channel zero and variations in this parameter are a greater percent of the photon energy than the gain, or gradient, at the low channel numbers that the iron fluorescence feature appears. Variations in the offset were observed over a single orbital period and over many days. The offset, determined by the center of the 10.2 keV line in this case, varied by $\sim$0.2 keV/day and $\sim$0.01 keV/orbit respectively. The daily variation was most likely a result of the satellite's pass through the

south atlantic anomaly. The relative period between the rotation of a fixed point on Earth and satellite precession was 0.3 percent different than the mean of the fitted period. The orbital variation in the offset consistently decreased for each time range and each detector. Electronics are temperature sensitive so the effect of sunrise and sunset were thought to affect the offset. A concave-down, second-order polynomial fit the orbital variation well with a χ^2 of 0.5. The specific cause of this feature was unidentified but it is likely a signature of typical orbital temperature fluctuations.

Correcting for variations in the offset would be accomplished by appending the program that calculates the gain function. Continuing the project would include determining the cause of the orbital variation. Correcting for the offset variations allows more accurate measurements of the iron fluorescence feature around 6.7 keV which is used in the determination of electron temperatures and the extent of thermal emission during solar flares. Solar flare temperatures provide insight into the methods of acceleration of coronal plasma, a highly theoretical field. Calibration projects allow the satellite to be used to the best of its resolution. Getting the most precise measurements from satellites justifies the high expenses of launch, and allows RHESSI to be effectively used far beyond the initial two year mission.

5

Acknowledgments

I would like to thank my advisor, Professor David Smith, for providing enthusiasm, wisdom, the opportunity, and support in this project and my education.

I would like to thank my mom, Kathy Diamond, for showing me the beauty of science and for supporting me, emotionally and financially, through my education.

6

References

Aschwanden, Markus. 2005. Physics of the Solar Corona. Springer-Praxis, Verlag.

Doschek, G. A., 2000. The Electron Temperature and Fine Structure of Soft X-Ray Solar Flares. High Energy Solar Physics: Anticipating HESSI ASP Conference Series, Vol. 206: 204-209.

Heirtzler, J. R., 2002. The Future of the South Atlantic Anomaly and Implication for Radiation Damage in Space. Journal of Atmospheric and Solar-Terrestrial Physics 64: 1701-1708.

Markwardt, C. B. 2008, "Non-Linear Least Squares Fitting in IDL with MPFIT," in proc. Astronomical Data Analysis Software and Systems XVIII, Quebec, Canada, ASP Conference Series, Vol. 411, eds. D. Bohlender, P. Dowler & D. Durand (Astronomical Society of the Pacific: San Francisco), p. 251-254

Phillips, K. J. II, Chifor, C., Dennis, B. R. 2006. RHESSI Observations of the Solar Flare Iron-Line Feature at 6.7 keV. The Astrophysical Journal 647: 1480-1490.

Priest, E. R. 2000. solar Flare Theory and the Status of Flare Understanding. High Energy

Solar Physics: Anticipating HESSI. ASP Conference Series 206: 13-26.

Lin, R. P. et al., 2002. The Reuven Ramaty High-Energy Solar Spectroscopic Imager (RHESSI). Solar Physics 210: 3-32.

Lyons, Louis. 1991. A Practical Guide to Data Analysis for Physical Science Students. Cambridge University Press.

Smith, D. M. et al., 2000. The HESSI Spectrometer. High Energy Solar Physics: Anticipating HESSI. ASP Conference Series 206: 92-101.

Tipler, Paul A., Llewellyn, Ralph A., 2002. Modern Physics, 4th Edition. W. H. Freemand and Company, New York.

——Note——

IDL procedures: obtain.pro, track_offset_mpfit.pro, troff_5min_mpfit.pro, fold_offsets_mpfit.pro, chi_5min.pro, and chi_5min_all.pro were created by the author to perform the analysis.